Theory and numerical simulations of defect ordering in irradiated materials

D. Walgraef*
Mechanical and Aerospace Engineering Department, University of California at Los Angeles, Los Angeles, California 90024

J. Lauzeral
Departemento de Fisica, Facultad de Ciencias Fisicas y Matematicas, Universidad de Chile, Santiago, Chile

N. M. Ghoniem
Mechanical and Aerospace Engineering Department, University of California at Los Angeles, Los Angeles, California 90024

(Received 14 September 1995; revised manuscript received 12 February 1996)

A general theory for the spatial ordering of immobile clustered defects in irradiated materials is presented here. A vectorial form for the Fourier transforms of perturbations in the concentration of point and clustered defects is derived. Linear stability analysis indicates that, under conditions appropriate for void growth (high temperature), instabilities leading to spatially ordered microstructure are driven by vacancy cluster density fluctuations, which extends the range of validity of previous conclusions for microstructure with no void present (e.g., low temperature). The crucial importance of collision-cascade-induced vacancy cluster formation is clearly shown. Amplitude equations of the Ginzburg-Landau type are derived and used to discuss the qualitative features of microstructure pattern formation in the post-bifurcation regime. This is accompanied by numerical analysis of the space-time rate equations to test the validity of the weakly nonlinear analysis. Evolution of one- and two-dimensional patterns of the microstructure is illustrated by examples of typical reactor and accelerator irradiation conditions. The quasistatic approximation used in the weakly nonlinear analysis is shown to be adequate only for short irradiation doses. At larger times, higher mode generation leads to a wavelength selection that is somewhat insensitive to the dose, as observed experimentally. The role of interstitial diffusion anisotropy is shown to be significant in the alignment of microstructural patterns in parallel orientation to the directions of high interstitial mobility, in agreement with experiments. [S0163-1829(96)03722-8]

I. INTRODUCTION

Numerous experimental observations on irradiated materials have shown systematically the existence of fully or partially ordered defect populations in materials under irradiation. The phenomenon appears to be generic, where various types of microstructures (e.g., voids, precipitates, vacancy clusters, stacking faults tetrahedra, gas bubbles, and interstitial atoms clusters) are spatially arranged in patterns of typical dimensions 2–3 orders of magnitude greater than the atomic spacing. Striking observations have shown complete spatial isomorphism between the periodic structure of defect distributions and that of the fundamental atomic lattice. These experimental observations are particularly true for the spatial ordering of bubble[1,2] and void defect structures.[3–5] Recently, detailed and systematic observations of defect ordering under ion-irradiated nickel and copper have shown the development of periodic defect walls.[6] Formation of the walls of defect clusters in polycrystalline and single-crystalline Cu and Ni were observed at medium temperatures and high irradiation doses. The experimental observations of Jaeger and co-workers have clearly demonstrated strong anisotropic arrangements of stacking fault tetrahedra and vacancy-type clusters in walls along the {100} planes of the fcc crystal lattice. Because of the equivalency between {100} planes, labyrinth structures were observed.[7] These arrangements show a periodicity of 60 nm, with the walls having a thickness of less than half the periodicity length, and defect-free zones are observed in between the walls. One of the significant observations is that the spatial wavelength is rather insensitive to temperature, dose, and displacement damage rate.

Based on the experimental findings, the following conditions appear to be necessary for the formation of ordered defect microstructures.

(1) Collision-cascade-induced clustering of vacancies into dislocation loops, perhaps directly during the collisional phase of cascade cooling.

(2) A bias for dislocations toward preferential obsorption of interstitials over vacancies.

(3) Some degree of anisotropy during the evolution of clustered defects. This could either be triggered by diffusional anisotropies of point defects, or by anisotropic elastic interaction between defect clusters during the latter stages of their evolution. Although these effects do not necessarily affect the shape of the clusters, they determine the symmetries of the cluster distributions and thus of the microstructure itself.

We have published a number of articles providing a coherent understanding of the phenomenon of irradiation-induced self-organization in metals.[8–10] In these articles, we addressed the various conditions for evolution of microstructural patterns under irradiation. In Ref. 8, a simplified model of the necessary ingredients for pattern formation is pre-

sented, where only vacancy clusters (loops) are considered in addition to two mobile point defect species (vacancies and interstitials). It is shown that the onset of spatial instability is controlled by a critical bifurcation parameter related to the ratio of the evolving vacancy loop density (ρ_L) and the static network dislocation density (ρ_N), modified by a function of the bias (B) and the fraction of point defects produced in vacancy clusters within the cascade (i.e. cascade collapse efficiency ϵ). The instability threshold condition is expressed as

$$\rho_L > \frac{\rho_N}{(\sqrt{B/\epsilon}-1)^2}. \tag{1}$$

In subsequent publications, more complex models for irradiation-induced patterning have been worked out. The effects of simultaneous clustering of interstitial loops, as well as point-defect diffusional anisotropies, were addressed in Ref. 9. Furthermore, our work in Ref. 10 focused on the influence of microstructure evolution on changes to the initial periodicity and selected patterns. Additionally, our previous work[10] incorporated the direct production of interstitial clusters in evolution equations. The work has so far been analytical, leading to a concrete yet qualitative description of the conditions needed for pattern formation.

These earlier works are based on the dynamic evolution of point and line defects only. Furthermore, the analytical results have been obtained by assuming that the evolution of the microstructure is sufficiently slow to justify a quasistatic approximation. Hence, to achieve a complete understanding of microstructure formation and evolution, one requires a study of the effect of the presence of volume defects such as voids or stacking fault tetrahedra in the dynamics, and a thorough analysis of the dynamics in the absence of any quasistatic approximation. It is the aim of the present work to address these questions, and is based on the following elements:

(1) It presents a further extension of our previous analysis in three important regards:

(a) Kinetic equations for the immobile microstructures are expanded further to include an additional equation for the growth of voids. Thus all relevant elements of clustered and immobile defect populations are treated (i.e., vacancy dislocation loops, interstitial dislocation loops, and voids).

(b) The dynamical equations for perturbations in defect populations are cast in a generalized vectorial form, which can encompass additional immobile elements of the microstructure.

(c) Destabilization of the void density population is analyzed.

(2) Since it is found that microstructure formation is governed by the instability of vacancy loop distribution, it remains to test the quasistatic approximation used up to now. This is done through the numerical analysis of the reduced version of the model, which is based on point and line defect evolution only. The main result of this analysis is that, although it may only be really justified for cold worked materials, the first part of the evolution is generally in agreement with the quasistatic approximation. Deviations occur at later stages, but are only quantitative and result in a slight decrease of the wavelength of the wall patterns, and in a sharpening of the walls. Another important result of this analysis is the major role played by diffusional anisotropy in the orientation of the walls.

In Sec. II, we present an expanded form of our rate theory model to include the void microstructure. This is followed by an analysis of dislocation and void dynamics in Sec. III. Conditions for the onset of microstructural instabilities are derived in Sec. IV. A weakly nonlinear analysis is presented in Sec. V leading to a discussion of amplitude equations for the growth, saturation, and selection of spatially organized microstructures. Numerical analysis of the dynamical model is presented in Sec. VI, leading to a discussion of pattern selection in one and two dimensions, in Secs. VII and VIII, respectively. Finally, conclusions are drawn in Sec. IX.

II. RATE THEORY MODEL OF MICROSTRUCTURE EVOLUTION

In order to account explicitly for the effect of direct interstitial loop production on the evolution of defect populations, including voids, we propose a rate theory dynamical model. Radiation-produced defects are represented by two equations for point defects, which are considered as mobile species and a set of equations describing the evolution of loops which are considered as immobile species. Since point defects are the only mobile components of the microstructure, their rate equations would include spatial operators. Immobile microstructures are represented by loops and voids as shown below:

$$\begin{aligned}
\partial_t c_i &= K(1-\epsilon_i) - \alpha c_i c_v + D_i \nabla^2 c_i - D_i c_i (Z_{iN}\rho_N + Z_{iV}\rho_V \\
&\quad + Z_{iI}\rho_I + Z_{iC}\rho_C), \\
\partial_t c_v &= K(1-\epsilon_v) - \alpha c_i c_v + D_v \nabla^2 c_v - D_v [Z_{vN}(c_v - \overline{c_{vN}})\rho_N \\
&\quad + Z_{vV}(c_v - \overline{c_{vV}})\rho_V + Z_{vI}(c_v - \overline{c_{vI}})\rho_I \\
&\quad + Z_{vC}(c_v - \overline{c_{vC}})\rho_C], \\
\partial_t \rho_I &= \left(\frac{2\pi N}{|\mathbf{b}|}\right)[\epsilon_i K + D_i Z_{iI} c_i - D_v Z_{vI}(c_v - \overline{c_{vI}})], \\
\partial_t \rho_V &= \frac{1}{|\mathbf{b}| r_V^0}\{\epsilon_v K - \rho_V [D_i Z_{iV} c_i - D_v Z_{vV}(c_v - \overline{c_{vV}})]\}, \\
\partial_t \rho_C &= \frac{(4\pi N_c)^2}{\rho_C}[D_v Z_{vC}(c_v - \overline{c_{vC}}) - D_i Z_{iC} c_i],
\end{aligned} \tag{2}$$

where c_v corresponds to the concentration of vacancies and c_i to interstitials. ρ_N is the network dislocation density, ρ_V the vacancy loop density, ρ_I the interstitial loop density, and ρ_C the void sink density ($\rho_C = 4\pi N_c R_c$, with N_c being the void number density and R_c the mean void radius). K, is the displacement damage rate, $\epsilon_i K$ is the interstitial loops production rate, ϵ_v is the cascade collapse efficiency, α is the recombination coefficient, $\mathbf{b}$ is the Burgers vector, r_V^0 is the mean vacancy loop radius, and Z... are the bias factors which will be approximated by $Z_{iN} = Z_{iI} = Z_{iV} = 1 + B$

and $Z_{vI}=Z_{vN}=Z_{vV}=Z_{vC}=Z_{iC}=1$. B is the excess network bias. c_{vN}, c_{vV}, c_{vI}, and c_{vC} are the concentrations of thermally emitted vacancies from network dislocations, vacancy and interstitial loops, and voids, respectively.

We shall now use the following scaling relations:

$$\lambda_v=D_vZ_{vN}\rho_N,\quad \overline{D_\cdot}=D_\cdot/\lambda_v,\quad \alpha/\lambda_v=\gamma,\quad P=\gamma K/\lambda_v,$$

$$\rho^*_{V,I}=\frac{\rho_{V,I}}{\rho_N},\quad x_{i,v}=\gamma c_{i,v},\quad \overline{x_{vN}}\ll\overline{x_{vV}}\simeq\overline{x_{vI}}\simeq\overline{x_{vC}}=\overline{x_{vL}}, \tag{3}$$

$$\mu=\frac{D_i}{D_v},\quad \tau=\lambda_v t,$$

$$\tau_I=\frac{b\alpha\rho_N}{2\pi N D_v},\quad \tau_V=br_v^0\rho_N\gamma,\quad \tau_C=\frac{\alpha\rho_N^2}{(4\pi N_c)^2D_v}.$$

Equations (2) can now be written in dimensionless form:

$$\begin{aligned}
\partial_\tau x_i&=P(1-\epsilon_i)-x_ix_v+\mu\overline{D_v}\nabla^2x_i\\
&\quad-\mu x_i[(1+B)(1+\rho_v^*+\rho_I^*)+\rho_c^*],\\
\partial_\tau x_v&=P(1-\epsilon_v)-\overline{x_{vL}}-x_ix_v+\overline{D_v}\nabla^2x_v\\
&\quad-(x_v-\overline{x_{vL}})(1+\rho_v^*+\rho_I^*+\rho_C^*),\\
\tau_I\partial_\tau\rho_I^*&=\epsilon_iP+\mu(1+B)x_i-(x_v-\overline{x_{vL}}),\\
\tau_V\partial_\tau\rho_V^*&=\epsilon_vP-\rho_V^*[\mu(1+B)x_i-(x_v-\overline{x_{vL}})],\\
\tau_C\partial_\tau\rho_c&=\frac{1}{\rho_C^*}[(x_v-\overline{x_{vL}})-\mu x_i].
\end{aligned}\tag{4}$$

Since point defect densities evolve much more rapidly than that of loops, they may, as usual, be adiabatically eliminated from the dynamics and their evolution related to that of loop densities. In the case of uniform defect densities, and ignoring recombination, we obtain

$$\begin{aligned}
(x_v^0-\overline{x_{vL}})&=\frac{P(1-\epsilon_v)-\Delta}{A_0},\\
x_i^0&=\frac{P(1-\epsilon_i)}{\mu(1+B)B_0},
\end{aligned}\tag{5}$$

where $\Delta=\overline{x_{vL}}-\overline{x_{vN}}\simeq\overline{x_{vL}}$, $A_0=1+\rho_V^0+\rho_I^0+\rho_C^0$, and $B_0=1+\rho_V^0+\rho_I^0+(\rho_C^0)/(1+B)$.

In order to study the evolution of nonuniform defect distributions and the eventual occurrence of microstructure formation, we also need to derive the evolution equations for inhomogeneous defect densities. We follow the same method as in Ref. 10, and define the nonuniform densities as

$$\begin{aligned}
&\delta x_i=x_i-x_i^0,\quad \delta x_v=x_v-(x_v^0-\overline{x_{vL}}),\\
&\delta\rho_V=\frac{\rho_V^*-\rho_V^0}{\rho_V^0},\quad \delta\rho_I=\frac{\rho_I^*-\rho_I^0}{\rho_I^0},\quad \delta\rho_C=\frac{\rho_C^*-\rho_C^0}{\rho_C^0},
\end{aligned}\tag{6}$$

where x_i^0, x_v^0, ρ_V^0, ρ_I^0, and ρ_C^0 are the uniform defect densities. On introducing these variables in system (4), point defect perturbations may easily be expressed as an expansion in powers of the loop density perturbations, which may be written, in vectorial form, as (cf. the Appendix)

$$\begin{aligned}
\delta\mathbf{x_q}=\Sigma_{n\geqslant1}&\int d\mathbf{k}\cdots\int d\mathbf{k}_{n-1}\\
&\times(-1)^{(n)}\mathbf{D}^{(n)}_{\mathbf{q},\ldots,\mathbf{k}_{n-1}}\mathbf{T_q}\delta\rho_{\mathbf{q}-\mathbf{k}}\cdots\delta\rho_{\mathbf{k_{n-1}}}.
\end{aligned}\tag{7}$$

III. DISLOCATION AND VOID DYNAMICS

The main result of Sec. II is that, due to the huge timescale difference between the evolution of point and line defects, the point defect densities may be expressed as functions of the line defect densities which govern the evolution of the whole system. This adiabatic elimination of point defect densities thus leads to the reduction of the dynamics to the dynamics of dislocation loops and void densities only. On defining $\overline{\epsilon}=\epsilon_v-\epsilon_i$, we obtain the following reduced kinetic equations for the uniform defect densities:

$$\begin{aligned}
\tau_I\partial_\tau\rho_I^0&=\epsilon_iP+\frac{P(1-\epsilon_i)}{B_0}-\frac{P(1-\epsilon_v)-\Delta}{A_0},\\
\tau_V\partial_\tau\rho_V^0&=\epsilon_vP-\left[\frac{P(1-\epsilon_i)}{B_0}-\frac{P(1-\epsilon_v)-\Delta}{A_0}\right]\rho_V^0,\\
\tau_C\partial_\tau\rho_C^0&=-\frac{1}{\rho_C^0}\left[\frac{P(1-\epsilon_i)}{(1+B)B_0}-\frac{P(1-\epsilon_v)-\Delta}{A_0}\right].
\end{aligned}\tag{8}$$

On the other hand, the evolution of nonuniform densities is given by the following equation, in Fourier space:

$$\begin{aligned}
\tau_V\partial_\tau\delta\rho_{V\mathbf{q}}&=-\frac{\epsilon_vP}{\rho_V^0}\,\delta\rho_{V\mathbf{q}}-[\mu(1+B)\,\delta x_{i\mathbf{q}}-\delta x_{V\mathbf{q}}]\\
&\quad-\int d\mathbf{k}\;\delta\rho_{V\mathbf{q}-\mathbf{k}}[\mu(1+B)\,\delta x_{i\mathbf{k}}-\delta x_{v\mathbf{k}}],\\
\tau_I\partial_\tau\delta\rho_{I\mathbf{q}}&=-(\epsilon_iP+\Gamma)\,\frac{\delta\rho_{I\mathbf{q}}}{\rho_I^0}+[\mu(1+B)\,\delta x_{i\mathbf{q}}-\delta x_{v\mathbf{q}}]\,\frac{1}{\rho_I^0},
\end{aligned}\tag{9}$$

$$\tau_C\partial_\tau\delta\rho_{C\mathbf{q}}=\frac{\delta\rho_{C\mathbf{q}}}{\rho_C^{0^2}}\overline{\Gamma}\left(2-\frac{\delta\rho_{C\mathbf{q}}}{1+\delta\rho_{C\mathbf{q}}}\right)-\frac{(\mu\,\delta x_{i\mathbf{q}}-\delta x_{v\mathbf{q}})}{\rho_C^{0^2}(1+\delta\rho_{C\mathbf{q}})},$$

with

$$\Gamma=\frac{P(1-\epsilon_i)}{B_0}-\frac{P(1-\epsilon_v)-\Delta}{A_0},$$

$$\overline{\Gamma}=\frac{P(1-\epsilon_i)}{(1+B)B_0}-\frac{P(1-\epsilon_v)-\Delta}{A_0},$$

and

$$\mu(1+B)\,\delta x_{i\mathbf{q}}-\delta x_{v\mathbf{q}}=\Sigma_{n\geqslant 1}(-1)^n\int d\mathbf{k}\cdots\int d\mathbf{k}_{n-1}\left(\frac{P(1-\epsilon_i)}{B_0}\,\frac{1}{B_q\cdots B_{k_{n-1}}}\,\Pi_{\mathbf{q}-\mathbf{k}}\cdots\Pi_{\mathbf{k}_{n-1}}\right.$$
$$\left.-\frac{P(1-\epsilon_v)-\Delta}{A_0}\,\frac{1}{A_q\cdots A_{k_{n-1}}}\,\Sigma_{\mathbf{q}-\mathbf{k}}\cdots\Sigma_{\mathbf{k}_{n-1}}\right), \tag{10}$$

$$\mu\,\delta x_{i\mathbf{q}}-\delta x_{v\mathbf{q}}=\Sigma_{n\geqslant 1}(-1)^n\int d\mathbf{k}\cdots\int d\mathbf{k}_{n-1}\left(\frac{P(1-\epsilon_i)}{(1+B)B_0}\,\frac{1}{B_q\cdots B_{k_{n-1}}}\,\Pi_{\mathbf{q}-\mathbf{k}}\cdots\Pi_{\mathbf{k}_{n-1}}\right.$$
$$\left.-\frac{P(1-\epsilon_v)-\Delta}{A_0}\,\frac{1}{A_q\cdots A_{k_{n-1}}}\,\Sigma_{\mathbf{q}-\mathbf{k}}\cdots\Sigma_{\mathbf{k}_{n-1}}\right). \tag{11}$$

Hence the loop dynamics may be cast in the vectorial form

$$\tau\partial_\tau\delta\boldsymbol{\rho}_{\mathbf{q}}=\mathbf{L}\delta\boldsymbol{\rho}_{\mathbf{q}}+\mathbf{M}\delta\mathbf{x}_{\mathbf{q}}+\int d\mathbf{k}\;\delta\boldsymbol{\rho}_{\mathbf{q}-\mathbf{k}}\mathbf{N}\delta\mathbf{x}_{\mathbf{k}}$$
$$+\int d\mathbf{k}\;\delta\boldsymbol{\rho}_{\mathbf{q}-\mathbf{k}}\mathbf{P}\delta\boldsymbol{\rho}_{\mathbf{q}-\mathbf{k}}+\cdots\,, \tag{12}$$

where

$$\tau=\begin{pmatrix}\tau_v & 0 & 0\\ 0 & \tau_l & 0\\ 0 & 0 & \tau_C\end{pmatrix}, \tag{13}$$

$$\mathbf{L}=\begin{pmatrix}-\dfrac{\epsilon_v P}{\rho_V^0} & 0 & 0\\ 0 & -\dfrac{(\epsilon_i P+\Gamma)}{\rho_I^0} & 0\\ 0 & 0 & \dfrac{2}{\rho_C^{0^2}}\,\overline{\Gamma}\end{pmatrix}, \tag{14}$$

$$\mathbf{M}=\begin{pmatrix}-\mu(1+B) & 1\\ \dfrac{\mu(1+B)}{\rho_I^0} & -\dfrac{1}{\rho_I^0}\\ -\dfrac{\mu}{\rho_C^{0^2}} & \dfrac{1}{\rho_C^{0^2}}\end{pmatrix}, \tag{15}$$

$$\mathbf{N}=\begin{pmatrix}-\mu(1+B) & 1\\ 0 & 0\\ \dfrac{\mu}{\rho_C^{0^2}} & -\dfrac{1}{\rho_C^{0^2}}\end{pmatrix}, \tag{16}$$

and

$$\mathbf{P}=\begin{pmatrix}0 & 0 & 0\\ 0 & 0 & 0\\ 0 & 0 & -\dfrac{\overline{\Gamma}}{\rho_C^{0^2}}\end{pmatrix}, \tag{17}$$

and supplemented with Eq. (7).

IV. ONSET OF SPATIAL INSTABILITY OF THE MICROSTRUCTURE

The evolution of the uniform line and volume defect densities may be studied with Eqs. (7) and (12). The addition element here, with respect to Ref. 10, is the presence of voids in the dynamics. Let us then first consider the growth rate of the void density. It is easy to see, when

$$\frac{P(1-\epsilon_i)}{(1+B)}>[P(1-\epsilon_v)-\Delta], \tag{18}$$

or when the net contribution of interstitials to the void growth rate exceeds the net contribution of vacancies to the void growth rate, that the void density continuously decreases. Although it may strongly depend on its initial condition, it will not affect the long-time behavior of the system. In this case, we are led back to the microstructure evolution problem studied in Ref. 10 with dislocation loops only. Of course, due to the weak coupling between the densities of loops and voids, any spatial instability in loop densities will eventually induce transient structures in the void density. This condition is consistent with the experimental condition of irradiation at low temperature (less than one-third of the melting point).

On the other hand, under conditions conducive to void growth (temperatures above one-third of the melting point), we have

$$\frac{P(1-\epsilon_i)}{(1+B)}<[P(1-\epsilon_v)-\Delta]. \tag{19}$$

In this case, the situation is quite different. Dimensional analysis of the evolution Eq. (8) shows that both loop and void densities increase with time or irradiation dose.

The stability of these uniform dislocation densities may now be analyzed through the linear part of the evolution equation for their inhomogeneous perturbations. This evolution is obtained by combining Eqs. (7) and (12), and its linear part reads

$$\tau\partial_\tau\delta\boldsymbol{\rho}_{\mathbf{q}}=[\mathbf{L}-\mathbf{M}\mathbf{D}_{\mathbf{q}}\mathbf{T}_{\mathbf{q}}\boldsymbol{\rho}^{\mathbf{0}}]\,\delta\boldsymbol{\rho}_{\mathbf{q}}=\boldsymbol{\Omega}_{\mathbf{q}}\delta\boldsymbol{\rho}_{\mathbf{q}}, \tag{20}$$

where

$$\mathbf{\Omega_q}=\begin{pmatrix} -\frac{\epsilon_V P}{\rho_V^0}+\Lambda_q\rho_V^0 & \Lambda_q\rho_I^0 & \overline{\Lambda}_q\rho_I^0 \\ -\Lambda_q\frac{\rho_V^0}{\rho_I^0} & \frac{(\epsilon_i P+\Gamma)}{\rho_I^0}-\Lambda_q & -\overline{\Lambda}_q\frac{\rho_C^0}{\rho_I^0} \\ \overline{\Lambda}_q\frac{\rho_V^0}{\rho_C^{0^2}} & \overline{\Lambda}_q\frac{\rho_I^0}{\rho_C^{0^2}} & \frac{2}{\rho_C^{0^2}}\overline{\Gamma}+\bar{\bar{\Lambda}}_q\frac{1}{\rho_C^0} \end{pmatrix}, \tag{21}$$

where

$$\Lambda_q=\frac{P(1-\epsilon_i)}{B_0B_q}-\frac{P(1-\epsilon_v)-\Delta}{A_0A_q}, \tag{22}$$

$$\overline{\Lambda}_q=\frac{P(1-\epsilon_i)}{(1+B)B_0B_q}-\frac{P(1-\epsilon_v)-\Delta}{A_0A_q}, \tag{23}$$

$$\bar{\bar{\Lambda}}_q=\frac{P(1-\epsilon_i)}{(1+B)^2B_0B_q}-\frac{P(1-\epsilon_v)-\Delta}{A_0A_q}. \tag{24}$$

Since the elements of the corresponding evolution matrix are time dependent, this situation prevents us from performing the usual stability analysis. Nevertheless, some insight into the behavior of the system may be obtained within the quasistatic approximation, as was done in our earlier work.[10] In this description, the time (or dose) appears just as a parameter, and one may obtain an instantaneous instability criterion. Effectively, when at least one eigenvalue of the evolution matrix acquires a positive real part, the corresponding eigenmode starts growing. Of course this approximation does not describe correctly the time evolution of the perturbations, but in similar problems it seems to predict the instability threshold quite accurately.

When the condition $[P(1-\epsilon_i)]/[(1+B)]<[P(1-\epsilon_v)-\Delta]<P(1-\epsilon_i)$ is satisfied, $\bar{\bar{\Lambda}}_q$ is limited by $B/(1+B)\rho_C^0$; and $[P(1-\epsilon_v)-\Delta]/A_qA_0B_0$; and $[P(1-\epsilon_i)]/[(1+B)B_0]/-[P(1-\epsilon_v)-\Delta]/A_0$ by $B/(1+B)\rho_C^0[P(1-\epsilon_v)-\Delta]/A_0B_0$, while for $[P(1-\epsilon_i)]/[(1+B)]<P(1-\epsilon_i)<(P(1-\epsilon_v)-\Delta)$, $[P(1-\epsilon_i)]/[(1+B)B_0]-[P(1-\epsilon_v)-\Delta]/A_0$ and $\bar{\bar{\Lambda}}_q$ are always negative. Hence the only instability possibility arises, once again, in the vacancy loop evolution.

Taking into account the fact that ρ_V^0/ρ_C^{02} and ρ_I^0/ρ_C^{02} decrease with time, and that $\tau_I\gg\tau_V$, the computation of the instability threshold is very similar to the computation made in Ref. 10, and we find that nonuniform defect densities start growing when the fraction of line defects corresponding to vacancy loops exceeds an instability threshold given, at the lowest order in ϵ_v, ϵ_i, B, and Δ, by

$$b=\frac{\rho_V^0}{1+\rho_I^0+\rho_V^0}>b_c=\frac{\rho_V^0}{1+\rho_I^0+\rho_V^0}\bigg|_c=\frac{2\sqrt{\epsilon_v B}}{B+\overline{\epsilon}+\frac{B}{1+B}\frac{\rho_C^0}{A_0}}, \tag{25}$$

where $\overline{\epsilon}=\epsilon_v-\epsilon_i+(\Delta/P)$. This instability occurs for a critical wave number given by

$$q_c^2=\frac{(1+\rho_I^0+\rho_V^0)(B-\overline{\epsilon})-\rho_C^0(2B+\overline{\epsilon})}{\overline{D_V}\left(B+\overline{\epsilon}+\frac{B}{1+B}\frac{\rho_C^0}{A_0}\right)}. \tag{26}$$

We immediately see that we recover the previous results[10] for $\rho_C^0=0$, and that the instability threshold is lowered by the presence of the void density. However, the instability occurs at finite q_c, when the following condition is satisfied:

$$\frac{\rho_C^0}{1+\rho_I^0+\rho_V^0}<\frac{B-\overline{\epsilon}}{2B+\overline{\epsilon}}, \tag{27}$$

which implies that microstructure formation occurs when, on one side, the bias exceeds the difference between the cascade collapse efficiency of vacancies and interstitials, and, on the other side, the uniform void density does not exceed a well-defined fraction of the total line defect density. Furthermore, with all material parameters fixed, one sees that an increase of line defect densities tends to decrease the wavelength of the critical microstructure, while an increase of the void density tends to increase it.

V. MICROSTRUCTURE STABILITY IN THE WEAKLY NONLINEAR REGIME

Close to the instability threshold of the steady uniform reference state of a nonlinear dynamical system, space-time separation occurs between stable and unstable modes, the characteristic scales of the latter being by far the largest. The stable modes may thus be eliminated adiabatically, and the dynamics reduced to the weakly nonlinear unstable mode dynamics, which governs the long-time evolution of the system and captures the asymptotic properties of the complete kinetic model in the vicinity of its bifurcation point. When this adiabatic elimination is performed, one usually obtains amplitude equations for the bifurcating solutions which have the structure of Landau or Landau-Ginzburg equations, and which have been discussed and analyzed at length in the literature in relation to the development of spatiotemporal patterns and self-organization phenomena in numerous physicochemical systems out of thermal equilibrium.

In the present case, our uniform reference state is time evolving, and we cannot perform this type of analysis. However, for weak nonlinearities, the void and loop dynamics can still be expressed as an expansion in the defect densities. Using Eqs. (7) and (12), one obtains.

$$\tau\partial_\tau\delta\boldsymbol{\rho}_{\mathbf{q}}=\boldsymbol{\Omega}_{\mathbf{q}}\delta\boldsymbol{\rho}_{\mathbf{q}}+\int d\mathbf{k}\,\mathscr{V}_{\mathbf{q},\mathbf{k}}\delta\boldsymbol{\rho}_{\mathbf{q}-\mathbf{k}}\delta\boldsymbol{\rho}_{\mathbf{k}}+\int d\mathbf{k}\int d\mathbf{k}_1\,\mathscr{U}_{\mathbf{q},\mathbf{k},\mathbf{k}_1}\delta\boldsymbol{\rho}_{\mathbf{q}-\mathbf{k}}\delta\boldsymbol{\rho}_{\mathbf{k}-\mathbf{k}_1}\delta\boldsymbol{\rho}_{\mathbf{k}_1}, \tag{28}$$

where

$$\mathscr{V}_{\mathbf{q},\mathbf{k}}=\mathbf{M}\mathbf{D}^{(2)}_{\mathbf{q},\mathbf{k}}\mathbf{T}_{\mathbf{q}}(\boldsymbol{\rho}^0)^2-\mathbf{N}\mathbf{D}_{\mathbf{q}}\mathbf{T}_{\mathbf{q}}\boldsymbol{\rho}^0+\mathbf{P} \tag{29}$$

and

$$\mathscr{U}_{\mathbf{q},\mathbf{k},\mathbf{k}_1}=-\mathbf{M}\mathbf{D}^{(3)}_{\mathbf{q},\mathbf{k},\mathbf{k}_1}\mathbf{T}_{\mathbf{q}}(\boldsymbol{\rho}^0)^3+\mathbf{N}\mathbf{D}^{(2)}_{\mathbf{q},\mathbf{k}}\mathbf{T}_{\mathbf{q}}(\boldsymbol{\rho}^0)^2. \tag{30}$$

Except in the quasistatic approximation, the usual procedure of diagonalization of the linear evolution matrix and the adiabatic elimination of the stable modes may not be performed on this dynamical system, due to the time dependence of the coefficients. However, since $\tau_C\gg\tau_I\gg\tau_V$, and since the elements of the matrices **M** and **N** are such that their lower components decrease with time or dose, it is easy to see from dimensional analysis that the dynamics is driven by the vacancy loops. For weak deviations from the uniform density, and at the leading order in $\epsilon=(b-b_c)/b_c$, and $(q-q_c)/q_c$, the vacancy loop density perturbation in Fourier space can be expressed as

$$\tau_{\mathbf{0}}\partial_\tau\delta\rho_{V_q}=\omega_q\delta\rho_{V_q}+\int dk\; v_{q_c}\delta\rho_{V_{q-k}}\delta\rho_{V_k}+\int dk\int dk_1 u_{q_c}\delta\rho_{V_{q-k}}\delta\rho_{V_{k-k_1}}\delta\rho_{V_{k_1}} \tag{31}$$

where

$$\omega_q=\frac{b-b_c}{b_c}-\xi_2^0\left(\frac{q^2-q_c^2}{q_c^2}\right)^2, \tag{32}$$

$$\tau_0=\tau_V\overline{\tau}=\frac{2\tau_V}{\sqrt{B\epsilon_v}(B+\overline{\epsilon})}, \tag{33}$$

$$v_{q_c}=\frac{\epsilon_v P\overline{\tau}}{\rho_V^0}+O\left(\frac{1}{A_0^2}\right), \tag{34}$$

$$u_{q_c}=\left(\frac{P(1-\epsilon_v)-\Delta}{A_0A_{q_c}^2}-\frac{P(1-\epsilon_i)}{B_0B_{q_c}^2}\right)(\rho_V^0)^2\overline{\tau}+O\left(\frac{1}{A_0}\right)\simeq\frac{\epsilon_v Pb_c\overline{\tau}}{\rho_V^0}+O\left(\frac{1}{A_0^2}\right), \tag{35}$$

$$\xi_0^2=\frac{\sqrt{1+B}(B-\overline{\epsilon})^2}{8B^3}. \tag{36}$$

Hence, as v^2/u decreases with irradiation dose, we may expect the same sequence of selected patterns as the one discussed in Ref. 9: bcc lattices at low irradiation doses and planar arrays at high irradiation doses.

Furthermore, the interstitial loop and void densities may be expressed as linear combinations of the eigenmodes of the linear evolution matrix. In this approximation ($\tau_C\gg\tau_I\gg\tau_V$), this leads to the following relations which express how they are linked to the vacancy loop density:

$$\delta\rho_{I_{q_c}}\simeq-\frac{\epsilon_v}{\rho_V^0\epsilon_i}\,\delta\rho_{V_{q_c}}, \tag{37}$$

$$\delta\rho_{C_{q_c}}\simeq\frac{(B+\overline{\epsilon})}{B(1+B)}\,\frac{\rho_V^0}{1+\rho_I^0+\rho_V^0}\,\delta\rho_{V_{q_c}}. \tag{38}$$

It is interesting to recall here that ρ_V^0 increases with dose while $\rho_V^0/(1+\rho_I^0+\rho_V^0)$ tends to a constant. As a result, the amplitudes of the inhomogeneities in the interstitial loop distribution decrease with dose, contrary to the amplitude of the inhomogeneities in the void density which are proportional to the amplitude of the vacancy loop microstructures.

The analysis performed here does not take into account the anisotropy of interstitial atom diffusion, which is related to the crystalline structure of the material. Effectively, it has been shown by us in Ref. 8 that the dislocation structures should be oriented parallel to the directions of high interstitial mobility. Hence, at low irradiation dose, the loop and void structures should be in parallel orientations with the underlying crystal lattice with the same symmetry, while at high irradiation dose (when $v^2/u\ll1$), the loop and void structures should consist of planar arrays. These arrays should nevertheless have their planes parallel to the crystalline axis. Up to now, most of the experimentally observed void lattices have been isomorphic with their host lattices.

VI. NUMERICAL SIMULATIONS

The weakly nonlinear analysis performed in preceding sections is valid in the quasistatic approximation close to threshold. Hence this analysis could become irrelevant for long irradiation times or high irradiation doses, when these approximations are supposed to break down. In such conditions, the numerical analysis of the dynamical model (2) remains the only way to test the validity of the weakly nonlinear analysis and to follow the microstructure evolution. Since it has been shown in the preceding sections that the presence of voids does not modify the character of the instability, we solved numerically the reduced version of this model where voids are absent.

Let us first describe the temporal evolution of the real part of the function $\Omega_+(q)$, which corresponds to the largest real part of the eigenvalues of the instantaneous linear evolution matrix. Recall that the modes for which this function is positive are unstable, and trigger the formation of defect microstructures. The evolution of $\mathrm{Re}\Omega_+(q)$ is presented in Figs. 1(a) and 1(b) for annealed ($\rho_N\simeq10^{13}$ m^{-2}) and cold worked ($\rho_N\simeq10^{15}$ m^{-2}) nickel in accelerator ($K=10^{-3}$ dpa s^{-1}), and in Fig. 1(c) for annealed nickel in reactor ($K=10^{-6}$ dpa s^{-1}) conditions. At short times, or small irradiation doses, all modes are stable and $\mathrm{Re}\Omega_+(q)$ is negative. Beyond a critical dose, a set of modes of wave numbers centered around $q_{\max}$, which corresponds to the maximum of $\mathrm{Re}\Omega_+(q)$, become unstable. Then $\mathrm{Re}\Omega_+(q_{\max})$ and $q_{\max}$ grow, as predicted by our previous analysis. However a time is finally reached where $\mathrm{Re}\Omega(q_{\max})$ stops growing and starts to decrease; the dispersion relation tends to flatten on the zero axis. The same behavior is also qualitatively observed for cold-worked and

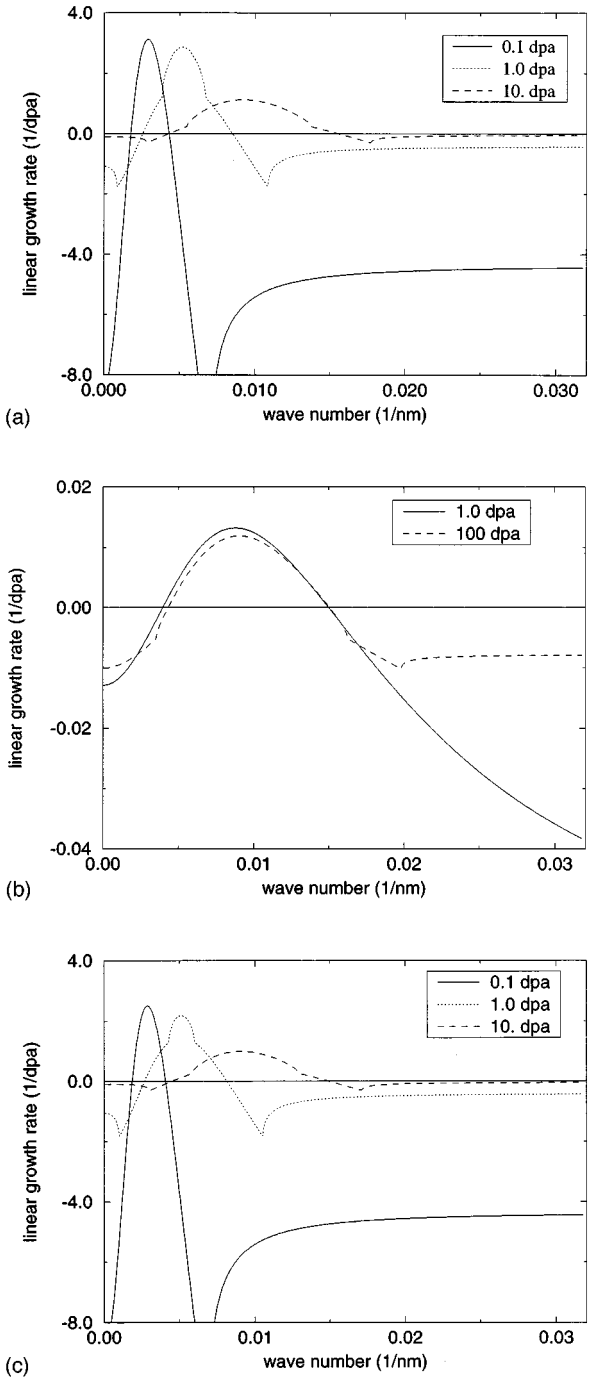

FIG. 1. Evolution of $\mathrm{Re}\Omega_+(q)$ (in the absence of voids) vs dose for annealed nickel under typical accelerator conditions and low temperatures ($\rho_N=10^{13}$ m^{-2}, $K=10^{-3}$ dpa s^{-1}, and $T=773$ K). (b) Evolution of $\mathrm{Re}\Omega_+(q)$ (in the absence of voids) vs dose for cold-worked nickel under typical accelerator conditions and low temperatures ($\rho_N=10^{15}$ m^{-2}, $K=10^{-3}$ dpa s^{-1}, and $T=773$ K). (c) Evolution of $\mathrm{Re}\Omega_+(q)$ (in the absence of voids) vs dose for annealed nickel under typical reactor conditions and low temperatures ($\rho_N=10^{13}$ m^{-2}, $K=10^{-6}$ dpa s^{-1}, and $T=773$ K).

annealed nickel, in accelerator ($T=773$ K, $K=10^{-3}$ dpa s^{-1}) or reactor conditions ($T=773$ K, $K=10^{-6}$ dpa s^{-1}), although the evolution is much slower for cold-worked nickel.

For high irradiation doses, both stable and unstable modes acquire comparable evolution time scales, and the adiabatic elimination of the stable modes is no longer appropriate. Furthermore, strong mode couplings and harmonic generation should be expected, leading to the breakdown of the weakly nonlinear analysis, except for cold-worked nickel, where the evolution of the linear growth rate curve $\mathrm{Re}\Omega_+(q)$ is sufficiently slow to guarantee time-scale separation between stable and unstable modes up to at least 10 dpa in accelerator conditions. Hence, for annealed nickel, the way to obtain accurate results from the kinetic model (2) consists of integrating it numerically.

The numerical integration of the evolution equations of defect densities has been performed in one and two spatial dimensions using an implicit Euler method. The four variable fields (point defects and loop densities) are initialized on the uniform state described in Ref. 9. Then an initial 1% noise is added to point defect densities, the initial time being chosen as the time where the linear stability analysis exhibits unstable modes. Since point defect densities evolve much more rapidly (by several orders of magnitude, as discussed in Ref. 8) than the loop densities, their evolution equations are solved implicitly, while the loop evolution equations are solved explicitly.

VII. WAVELENGTH SELECTION IN ONE DIMENSION

In one spatial dimension, a numerical system consisting of 512 cells is considered, and the spatial grid size is chosen in such a way that one wavelength corresponds roughly to 25 cells, and the boundary conditions are no flux. The integration is performed for several typical irradiation and materials conditions with respect to the temperature (low temperature $T=500°$ or high temperature $T=700°$), the irradiation intensity (accelerator conditions $K=10^{-3}$ dpa s^{-1} or reactor conditions $K=10^{-6}$ dpa s^{-1}) and the network dislocation density of the irradiated material (cold-worked nickel $\rho_N=10^{15}$ m^{-2} or annealed nickel $\rho_N=10^{13}$ m^{-2}). Under all conditions, our numerical simulations confirm the results of the linear stability analysis. In Table I we give the parameters used for the numerical analysis, while in Table II we present a summary of principal results: stability, critical dose, and critical wavelength.

Let us now qualitatively describe the process of microstructure formation and evolution as a result of the numerical analysis. Characteristic evolutions of the vacancy loop concentration are represented in Fig. 2, for annealed nickel under typical accelerator conditions and low temperature, and in Fig. 3 for cold-worked nickel under typical accelerator conditions and low temperature as a function of space and at different irradiation doses. Since the evolution of other variables is very similar, we do not represent them here. During early times, or low dose, unstable modes grow, giving rise to a more or less periodic structure. A wavelength adjustment occurs in intermediate periods. Finally, during late periods, or higher dose, the vacancy loop concentration increases strongly in very localized regions of the material, while it goes down almost everywhere else; the wavelength of the structure remains almost unchanged. The microstructure evolution is qualitatively similar in other irradiation conditions, although the time scale of the evolution may be different. This evolution is, for example, much slower in reactor conditions, where the irradiation is much less intense ($K=10^{-6}$

TABLE I. Material parameters for nickel.

Parameter	Symbol	Value	Units
Vacancy diffusion	D_v	$6\times10^{-5}e^{-1.3\ \mathrm{eV}/k_BT}$	$\mathrm{m^2\ s^{-1}}$
Interstitial diffusion	D_i	$10^{-7}e^{-0.3\ \mathrm{eV}/k_BT}$	$\mathrm{m^2\ s^{-1}}$
Equilibrium vacancy concentration	c_v^e	$e^{-1.6\ \mathrm{eV}/k_BT}$	
Stacking fault energy	γ_{sf}	9.4×10^{16}	$\mathrm{eV\ m^{-2}}$
Shear modulus	$\mu/(1-\nu)$	8×10^{10}	$\mathrm{Pa\ m^{-2}}$
Burgers vector	b	2.5×10^{-10}	m
Atomic volume	Ω	1.206×10^{-29}	$\mathrm{m^3}$
Network bias excess	B	0.1	
Loop/network bias excess	ΔB	0.005	
Initial vacancy loop radius	r_v^0	1.5×10^{-9}	m
Network dislocation density	ρ_n	10^{13}–10^{15}	$\mathrm{m^{-2}}$
Displacement damage rate	K	10^{-6}–10^{-3}	$\mathrm{dpa\ s^{-1}}$
Cascade collapse efficiency	ϵ	0.01–0.1	
Interstitial loop density	N	10^{20}–10^{22}	$\mathrm{m^{-3}}$
Temperature	T	773–973	K

$\mathrm{dpa\ s^{-1}}$), while the instability threshold is not very different (cf. Table II).

To characterize the wavelength selection phenomenon better, let us now describe the spectrum evolution (see Figs. 4 and 5). After a short irradiation time, the stable modes generated by the initial noise decrease, and a peak centered on the $q_{\max}$ wave vector is formed. This peak then continues to grow and is shifted toward slightly higher values of q. During the remaining time, another kind of evolution occurs; the main peak does no longer evolves, but its harmonics are successively generated. Hence the wavelength of the pattern no longer evolves, in agreement with Jaeger's observations,[6] while its profile strongly sharpens.

We can thus summarize the microstructure evolution in one-dimensional systems as follows. During early irradiation times, linear terms are responsible for wavelength selection. Selected modes rapidly grow. As time proceeds, the eigenvalues associated with the stable modes go to zero. This effect, combined with the presence of nonlinear terms, triggers the generation of harmonics of the initial unstable modes. These harmonics are responsible for sharpening of the loop density profile, or, in other words, of the accumulation of defects in very localized, although regularly spaced, regions.

VIII. PATTERN SELECTION AND ANISOTROPY EFFECTS IN TWO DIMENSIONS

The study of two-dimensional patterns has been performed on a (128×128) grid with periodic boundary conditions. The evolution presents the same characteristics as for one-dimensional systems, as far as the wavelength and the coarsening of the loop distributions are concerned. With respect to the symmetry of the structures, the weakly nonlinear analysis predicts a final wall three-dimensional (3D) or striped (2D) structure. On the other hand, and in other extended pattern forming systems, striped structures usually present a lack of orientational order, due to the presence of topological defects. It is only in anisotropic systems that regular parallel rolls or stripes may be observed.[11]

This behavior is also observed here, as illustrated in Fig. 6. Effectively, for isotropic point defect diffusion, the structure evolves toward mosaiclike patterns, with no well-defined orientation for the high loop concentration bands. The final structure resembles more regularly spaced defect clusters. However, in the case of anisotropic interstitial diffusion, well-defined bands are obtained, in parallel orientation with the high interstitial mobility, in agreement with our previous analysis.[8] Thus we have confirmation here that the anisotropies triggered by the crystalline structure of the material are essential in determination of the orientation of the microstructures, as observed in experiments.[6,7]

From this observation, and our previous analysis showing that the most unstable wave vectors are perpendicular to the high-mobility directions of the interstitials, we may thus infer the following scenarios for three-dimensional self-organization of loops. If the interstitial mobility is maximum for one set of planes, the defect microstructure should evolve toward regularly spaced walls parallel to these planes. If the interstitial mobility is maximum for two sets of planes, the

TABLE II. Numerical results for one-dimensional systems.

ρ_N ($\mathrm{m^{-2}}$)	K ($\mathrm{dpa\ s^{-1}}$)	Instability	Critical dose (dpa)	q_c ($\mathrm{m^{-1}}$)	q_{selected} ($\mathrm{m^{-1}}$)
10^{13}	10^{-3}	yes	0.025	1.3×10^7	3.65×10^7
10^{13}	10^{-6}	yes	0.03	1.4×10^7	3.9×10^7
10^{15}	10^{-3}	yes	$\cong$0 dpa	5.4×10^7	6.2×10^7
10^{15}	10^{-6}	no			

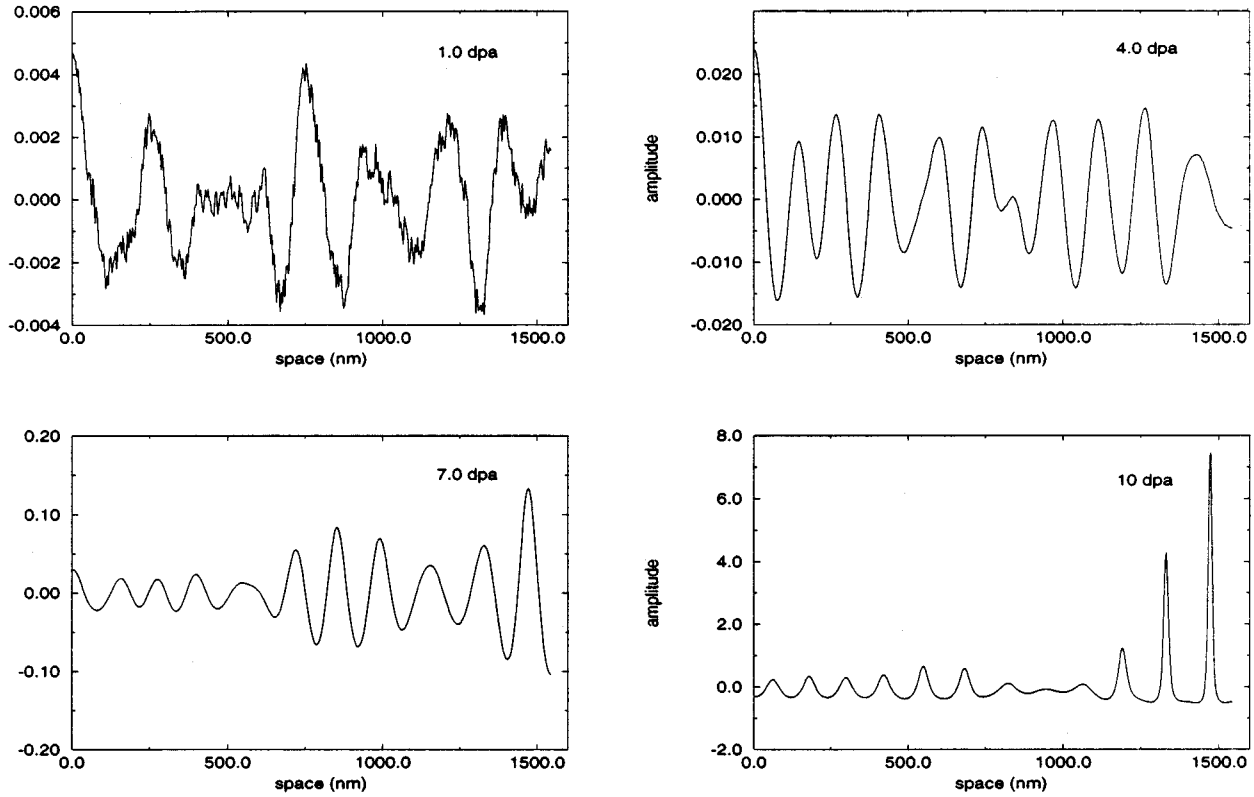

FIG. 2. Snapshots of the one-dimensional evolution of the amplitude of the vacancy loops microstructure ($\delta\rho_V$) in space at different irradiation doses for annealed nickel under typical accelerator conditions and low temperatures ($\rho_N = 10^{13}$ m^{-2}, $K = 10^{-6}$ dpa s^{-1}, and $T = 773$ K).

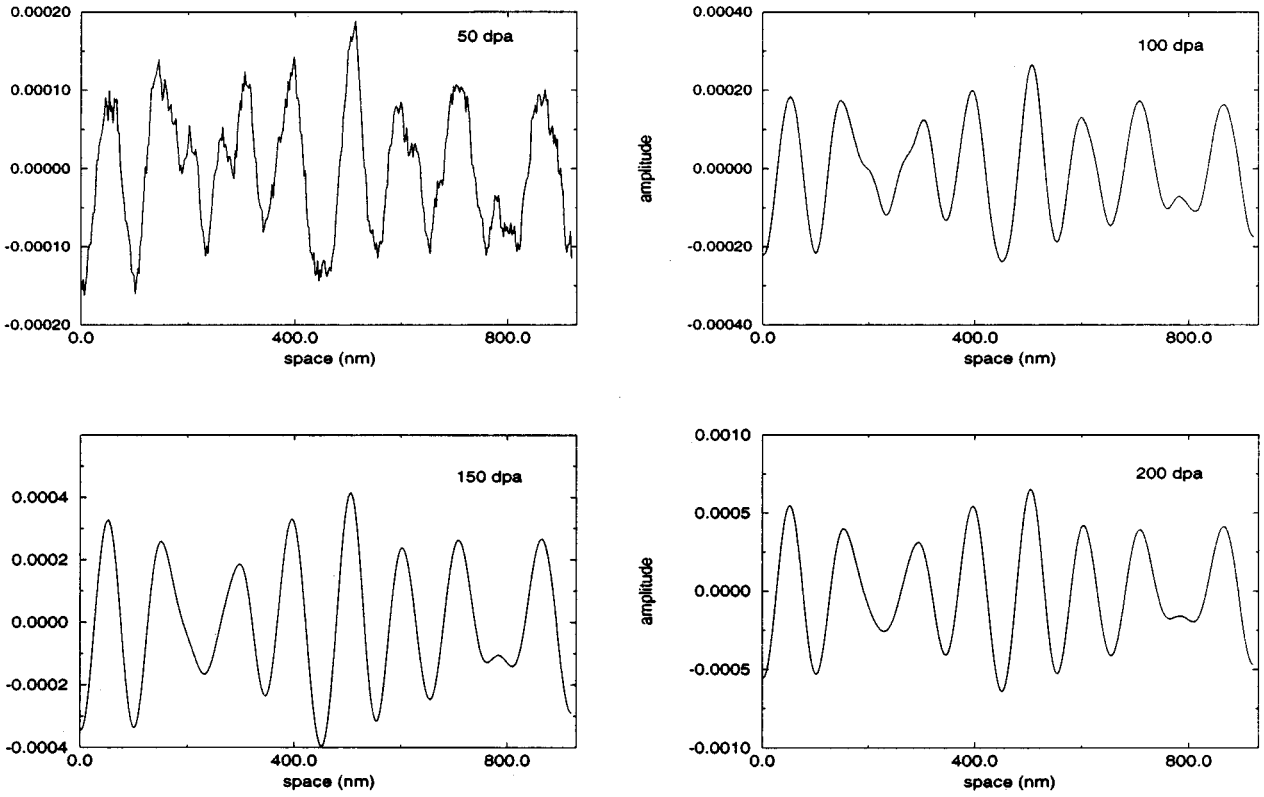

FIG. 3. Snapshots of the one-dimensional evolution of the amplitude of the vacancy loop microstructure ($\delta\rho_V$) in space at different irradiation doses for cold-worked nickel under typical accelerator conditions and low temperatures ($\rho_N = 10^{15}$ m^{-2}, $K = 10^{-3}$ dpa s^{-1}, and $T = 773$ K).

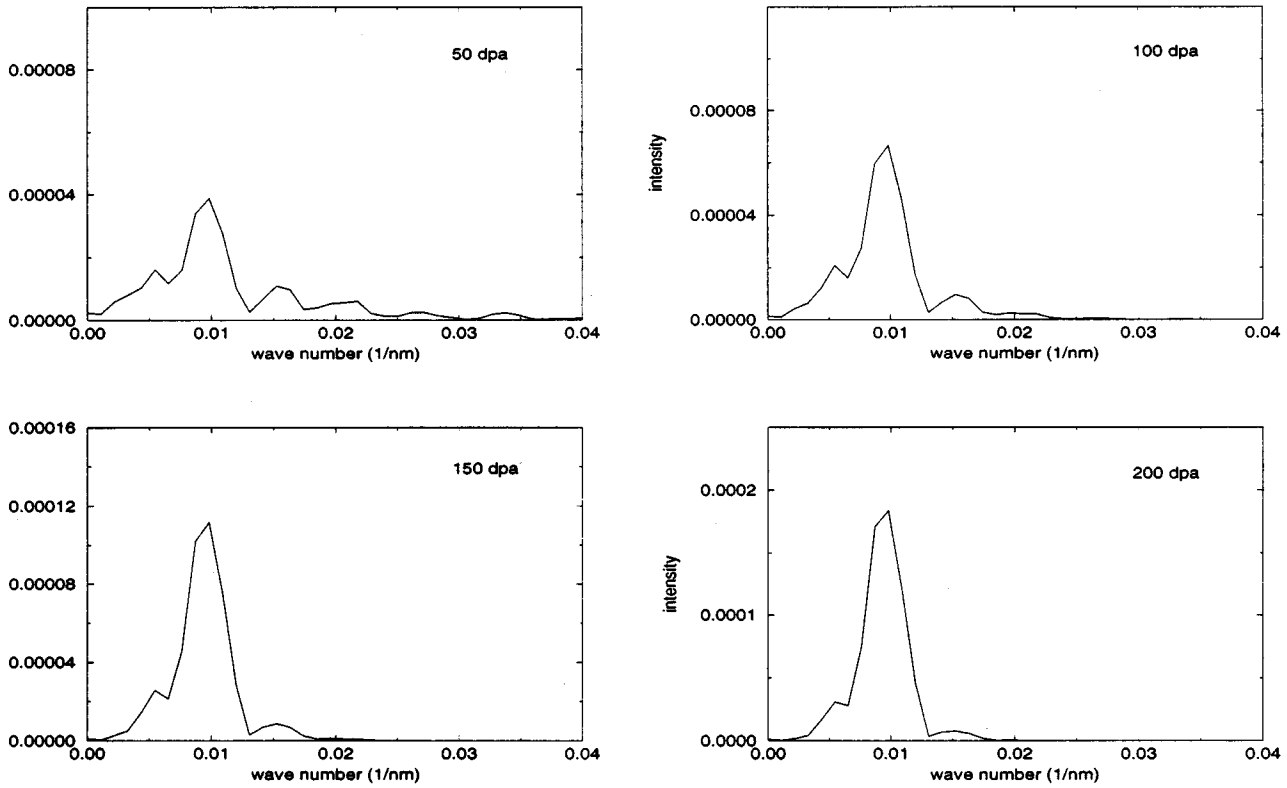

FIG. 4. Snapshots of the evolution of the spectrum (Fourier transform) of the amplitude of the vacancy loop microstructure presented in Fig. 2.

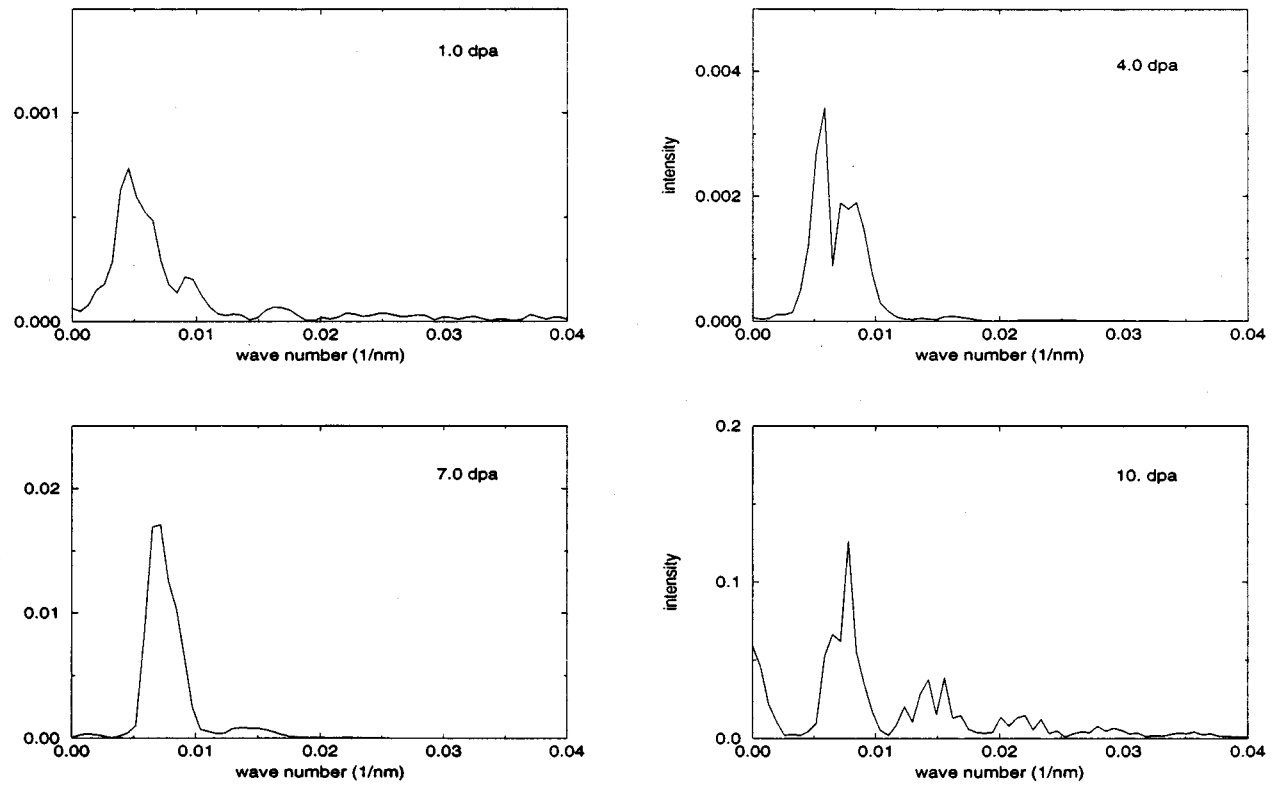

FIG. 5. Snapshots of the evolution of the spectrum (Fourier transform) of the amplitude of the vacancy loop microstructure presented in Fig. 3.

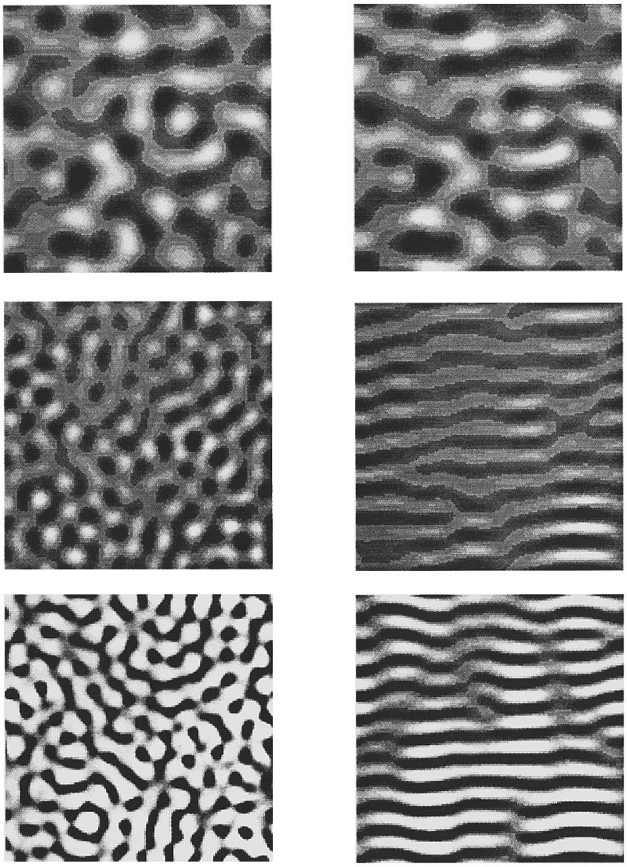

FIG. 6. Snapshots of the two-dimensional evolution of the amplitude of the vacancy loop microstructure ($\delta\rho_V$) in space at different irradiation doses for annealed nickel under typical accelerator conditions and low temperatures ($\rho_N=10^{13}$ m^{-2}, $K=10^{-6}$ dpa s^{-1}, and $T=773$ K) in the case of isotropic point defect diffusion (left column) (the dose increases from 1 dpa in the upper graph to 20 dpa in the lower graph), and with a 1% anisotropy in the interstitials diffusion coefficient (right column) (the dose increases from 1 dpa in the upper graph to 20 dpa in the lower graph).

defect microstructure should evolve toward a labyrinthic structure formed of domains of walls parallel to one or the other set of high mobility planes (cellular or bimodal structures are effectively ruled out by scalar nonlinearities[11]). If the interstitial mobility is maximum in one direction, say z, the most unstable wave vectors will be isotropically distributed in the plane perpendicular to the easy axis, say the (x,y) plane. Hence the resulting loop distribution should not vary in the z direction, but will in the (x,y) planes where it should present the same microstructure as the ones obtained in two-dimensional isotropic systems and presented in Fig. 6.

IX. SUMMARY AND CONCLUSIONS

A comprehensive theoretical framework for the analysis of spatial instabilities in the microstructure of irradiated materials is presented in this paper. The work is based on the well-established rate theory of microstructure evolution under irradiation, and is pursued both qualitatively and numerically to ascertain the main processes leading to pattern selection. Throughout this work, we emphasize conditions which are consistent with experimental observations, for the accuracy of the spatially organized microstructure.

The kinetic model described here is based upon the well-established rate theory of microstructure evolution. The model contains space-time rate equations for mobile point defects (vacancies and self-interstitials), with anisotropic diffusion for only the interstitial population. It also contains coupled space-independent rate equations for the densities of dislocation loops (represented by vacancy and interstitial loops), as well as voids. A compact vestorial form is derived for the Fourier components of perturbations in the densities of point defects, as well as clustered defects. The onset of spatial instabilities is analyzed through the linear part of the derived evolution equations. It is shown that, even when voids are present at high temperature, the spatial instabilities are driven by perturbations in the vacancy cluster (loop) density. Cascade-induced vacancy cluster densities must reach a critical value to induce the instability. This critical concentration is determined by the initial microstructure (i.e., annealed versus cold worked), the dislocation bias, and the cascade collapse efficiency. Numerical simulation verify the analytical conclusions, and show that a spatially organized defect microstructure is difficult to obtain for an initially cold-worked material.

Stability analysis in the weakly nonlinear regime is based on a derivation of density perturbations for the Fourier components of immobile defects, by invoking a quasistatic approximation. With this approximation, a Ginzburg-Landau-type amplitude equation is recovered, with time- (dose-) dependent coefficients that are slowly varying. Qualitative conclusions of pattern selection in the post bifurcation regime are made, to show phase transitions leading to the eventual formation of wall defect structures, with a wavelength that is decreasing with the irradiation dose.

Direct numerical simulations of the underlying kinetic model have largely confirmed the qualitative conclusions drawn on the basis of the weakly nonlinear analysis in the quasistatic approximation. However, the wavelength of the emerging patterns is shown to be somewhat insensitive to the irradiation dose, in agreement with experimental observations, because of higher-order harmonic generation at larger irradiation times. Numerical simulations have been performed for both cold-worked and annealed nickel under typical accelerator ($K=10^{-3}$ dpa s^{-1}) and reactor ($K=10^{-6}$ dpa s^{-1}) conditions. It is shown that during early irradiation times, linear terms controlled by the the critical vacancy cluster density, the cascade collapse efficiency, and the dislocation bias are responsible for wavelength selection. As time proceeds, eigenmodes associated with stable components decay, while nonlinear terms trigger a higher harmonic generation of unstable modes. The final effect is a rapid sharpening of the concentration of immobile defects into walls, with very few left in between.

Our weakly nonlinear analysis predicts a final wall (in 3D) or striped (in 2D) defect structures. Numerical simulations verify these conclusions in two-dimensional systems, where striped defect wall arrangements, with no preferred direction, are obtained when interstitial diffusion is assumed isotropic. On the other hand, only 1% anisotropy in the diffusion coefficient of self-interstitials along a preferred direc-

tion [i.e., (100)] is shown to result in significant alignment of clustered defects along (100) directions, in agreement with Jaeger's experimental observations. It is therefore concluded that a small degree of interstitial atom diffusional anisotropy is needed to result in significant alignment of clustered defects along (100) directions.

In summary, the necessary ingredients for the kinetic rate theory model to be consistent with experimental observations are three. These are (1) an excess bias of dislocations towards interstitial atom absorption; (2) a fraction of vacancies to be produced directly in clusters, as a result of collision cascades; and (3) a small degree of interstitial diffusional anisotropy.

ACKNOWLEDGMENTS

Financial assistance through Grant No. SC1*-CT092-0006 of the Commission of the European Union, through NATO Grant No. CRG-931365, and through a travel grant from the Belgian National Fund for Scientific Research is gratefully acknowledged. This work has also benefited from the support of the DOE/OFE through Grant No. DE-FG03-91ER54115 with UCLA. D.W. received support from the FNRS (Belgium).

APPENDIX

In this appendix, we give more details on the adiabatic elimination of the point defect densities. On introducing the perturbations to the uniform defect densities defined by the relations (6) in the dynamical system (4), and neglecting the time derivatives of the point defect densities (since $\tau_C \gg \tau_I \gg \tau_V \gg 1$), one obtains, in Fourier space,

$$\begin{aligned}
\delta x_{i,\mathbf{q}} &= -\frac{P(1-\epsilon_i)}{\mu(1+B)B_0B_q}\left(\rho_V^0\delta\rho_{v\mathbf{q}}+\rho_I^0\delta\rho_{I\mathbf{q}}+\frac{\rho_C^0}{1+B}\,\delta\rho_{C\mathbf{q}}\right)\\
&\quad-\int d\mathbf{k}\,\frac{1}{B_q}\,\delta x_{i,\mathbf{k}}\Big(\rho_V^0\delta\rho_{V\mathbf{q}-\mathbf{k}}+\rho_I^0\delta\rho_{I\mathbf{q}-\mathbf{k}}\\
&\quad+\frac{\rho_C^0}{1+B}\,\delta\rho_{C\mathbf{q}-\mathbf{k}}\Big),\\
\delta x_{v,\mathbf{q}} &= -\frac{P(1-\epsilon_v)-\Delta}{A_0A_q}\,(\rho_V^0\delta\rho_{V\mathbf{q}}+\rho_I^0\delta\rho_{I\mathbf{q}}+\rho_C^0\delta\rho_{C\mathbf{q}})\\
&\quad-\int d\mathbf{k}\,\frac{1}{A_q}\,\delta x_{v,\mathbf{k}}(\rho_V^0\delta\rho_{V\mathbf{q}-\mathbf{k}}+\rho_I^0\delta\rho_{I\mathbf{q}-\mathbf{k}}\\
&\quad+\rho_C^0\delta\rho_{C\mathbf{q}-\mathbf{k}}),
\end{aligned}\tag{A1}$$

where $B_q=B_0+q^2\overline{D_v}/(1+B)$ and $A_q=A_0+q^2\overline{D_v}$. On defining $\Pi_{\mathbf{q}}$ as $\rho_V^0\delta\rho_{V\mathbf{q}}+\rho_I^0\delta\rho_{I\mathbf{q}}+\rho_C^0/(1+B)\,\delta\rho_{C\mathbf{q}}$, and $\Sigma_{\mathbf{q}}$ as $\rho_V^0\delta\rho_{V\mathbf{q}}+\rho_I^0\delta\rho_{I\mathbf{q}}+\rho_C^0\delta\rho_{C\mathbf{q}}$, these equations may be simplified as

$$\begin{aligned}
\delta x_{i,\mathbf{q}} &= -\frac{P(1-\epsilon_i)}{\mu(1+B)B_0B_q}\,\Pi_{\mathbf{q}}-\int d\mathbf{k}\,\frac{1}{B_q}\,\delta x_{i,\mathbf{k}}\Pi_{\mathbf{q}-\mathbf{k}}\\
\delta x_{v,\mathbf{q}} &= -\frac{P(1-\epsilon_v)-\Delta}{A_0A_q}\,\Sigma_{\mathbf{q}}-\int d\mathbf{k}\,\frac{1}{A_q}\,\delta x_{v,\mathbf{k}}\Sigma_{\mathbf{q}-\mathbf{k}}.
\end{aligned}\tag{A2}$$

Since the coefficients of the linear terms are small, these equations may be solved by an iteration procedure, which leads to the following series expansion in $\Pi_{\mathbf{q}}$ and $\Sigma_{\mathbf{q}}$:

$$\begin{aligned}
\delta x_{i,\mathbf{q}} &= -\frac{P(1-\epsilon_i)}{\mu(1+B)B_0B_q}\left[\Pi_{\mathbf{q}}+\int dk\,\frac{1}{B_k}\,\Pi_{\mathbf{q}-\mathbf{k}}\Pi_{\mathbf{k}}-\int d\mathbf{k}\int d\mathbf{k}'\,\frac{1}{B_kB_{k'}}\,\Pi_{\mathbf{q}-\mathbf{k}}\Pi_{\mathbf{k}-\mathbf{k}'}\Pi_{\mathbf{k}'}+\cdots\right]\\
\delta x_{v,\mathbf{q}} &= \frac{P(1-\epsilon_v)-\Delta}{A_0A_q}\left[\Sigma_{\mathbf{q}}+\int d\mathbf{k}\,\frac{1}{A_k}\,\Sigma_{\mathbf{q}-\mathbf{k}}\Sigma_{\mathbf{k}}-\int d\mathbf{k}\int d\mathbf{k}'\,\frac{1}{A_kA_{k'}}\,\Sigma_{\mathbf{q}-\mathbf{k}}\Sigma_{\mathbf{k}-\mathbf{k}'}\Sigma_{\mathbf{k}'}+\cdots\right].
\end{aligned}\tag{A3}$$

Nonuniform point defect densities may thus be expressed in terms of linear and nonlinear combinations of line and volume defect densities. The introduction of these expressions, limited to the first significant nonlinear contributions, in the kinetic equations for line and volume defects, will thus provide a first reduction of the dynamics (4). In order to simplify the manipulations, Eq. (A3) may be cast in the vectorial form

$$\begin{aligned}
\delta\mathbf{x}_{\mathbf{q}} &= \Big[-\mathbf{D}_{\mathbf{q}}\delta\rho_{\mathbf{q}}+\int d\mathbf{k}\;\mathbf{D}_{\mathbf{q}}\mathbf{D}_{\mathbf{k}}\delta\rho_{\mathbf{q}-\mathbf{k}}\delta\rho_{\mathbf{k}}\\
&\quad-\int d\mathbf{k}\int d\mathbf{k}'\,\mathbf{D}_{\mathbf{q}}\mathbf{D}_{\mathbf{k}}\mathbf{D}_{\mathbf{k}'}\,\delta\rho_{\mathbf{q}-\mathbf{k}}\delta\rho_{\mathbf{k}-\mathbf{k}'}\delta\rho_{\mathbf{k}'}+\cdots\Big]\mathbf{T}_{\mathbf{q}},
\end{aligned}\tag{A4}$$

where

$$\delta\mathbf{x}_{\mathbf{q}}=\begin{pmatrix}\delta x_{i,\mathbf{q}}\\ \delta x_{v,\mathbf{q}}\end{pmatrix},\tag{A5}$$

$$\mathbf{T}_{\mathbf{q}}=\begin{pmatrix}\dfrac{P(1-\epsilon_i)}{\mu(1+B)B_0}\\[2ex] \dfrac{P(1-\epsilon_v)-\Delta}{A_0}\end{pmatrix},\tag{A6}$$

$$\mathbf{D}_{\mathbf{q}}=\begin{pmatrix}\dfrac{1}{B_q} & 0\\[2ex] 0 & \dfrac{1}{A_q}\end{pmatrix},\tag{A7}$$

and

$$\delta\boldsymbol{\rho}_{\mathbf{q}}=\begin{pmatrix}\Pi_{\mathbf{q}} & 0\\ 0 & \Sigma_{\mathbf{q}}\end{pmatrix}, \tag{A8}$$

or

$$\delta\boldsymbol{\rho}_{\mathbf{q}}=\boldsymbol{\rho}^{\mathbf{0}}\delta\boldsymbol{\rho}_{\mathbf{q}}, \tag{A9}$$

with

$$\boldsymbol{\rho}^{\mathbf{0}}=\begin{pmatrix}\rho_V^0 & \rho_I^0 & \dfrac{\rho_C^0}{1+B}\\ \rho_V^0 & \rho_I^0 & \rho_C^0\end{pmatrix} \tag{A10}$$

and

$$\delta\boldsymbol{\rho}_{\mathbf{q}}=\begin{pmatrix}\delta\rho_{V\mathbf{q}}\\ \delta\rho_{I\mathbf{q}}\\ \delta\rho_{C\mathbf{q}}\end{pmatrix}. \tag{A11}$$

Since the matrix $\mathbf{D}_{\mathbf{q}}$ is diagonal, Eq. (7) may finally be rewritten as

$$\delta\mathbf{x}_{\mathbf{q}}=\Sigma_{n\geqslant 1}\int d\mathbf{k}\cdots\int d\mathbf{k}_{n-1} \times(-1)^{(n)}\mathbf{D}^{(n)}_{\mathbf{q},\ldots,\mathbf{k}_{n-1}}\mathbf{T}_{\mathbf{q}}\delta\rho_{\mathbf{q}-\mathbf{k}}\cdots\delta\rho_{\mathbf{k}_{\mathbf{n-1}}}, \tag{A12}$$

where

$$\mathbf{D}^{(n)}_{\mathbf{q},\ldots,\mathbf{k}_{n-1}}=\begin{pmatrix}\dfrac{1}{B_q\ldots B_{k_{n-1}}} & 0\\ 0 & \dfrac{1}{A_{\mathbf{q}}\ldots A_{k_{n-1}}}\end{pmatrix}. \tag{A13}$$

This expression also allows an easy computation of the expressions $\mu(1+B)\delta x_{i\mathbf{q}}-\delta x_{v\mathbf{q}}$ and $\mu\delta x_{i\mathbf{q}}-\delta x_{v\mathbf{q}}$, which enter into the loop and void dynamics.

*Permanent address: Center for Nonlinear Phenomena and Complex Systems, Free University of Brussels, CP 231, B-1050 Brussels, Belgium.

[1] S. Sass and B. L. Gyre, Philos. Mag. **27**, 1447 (1973).
[2] P. B. Johnson, D. J. Mazey, and J. H. Evans, Radiat. Eff. **78**, 147 (1983).
[3] J. H. Evans, Nature **29**, 403 (1971); Radiat. Eff. **10**, 55 (1971).
[4] G. L. Kulcinski, J. L. Brimhall, and H. E. Kissinger, *Proceedings of the 1971 International Conference on Radiation-Induced Voids in Metals, Albany, NY* (USAEC, Washington DC, 1972), p. 465.
[5] F. W. Wiffen, *Proceedings of the 1971 International Conference on Radiation-Induced Voids in Metals* (Ref. 4), p. 386.
[6] W. Jaeger, P. Ehrhart and W. Schilling, Solid State Phenom. **3-4**, 297 (1988); Radiat. Eff. Def. Solids **113**, 201 (1990).
[7] W. Jaeger and H. Trinkaus, J. Nucl. Mater. **205**, 394 (1993).
[8] D. Walgraef and N. M. Ghoniem, Phys. Rev B **39**, 8867 (1989).
[9] N. M. Ghoniem and D. Walgraef, Model. Simul. Mater. Sci. Eng. **1**, 569 (1993).
[10] D. Walgraef and N. M. Ghoniem, Phys. Rev. B **52**, 3951 (1995).
[11] D. Walgraef, in *Reactive Phase Formation at Interfaces and Diffusion Processes*, edited by Y. Limoge and J. L. Bocquet, Materials Science Forum Vol. 155-156 (Trans Tech, Aedermannsdorf, Switzerland, 1994), pp. 401–408.